AGU PUBLICATIONS

Journal of Advances in Modeling Earth Systems

RESEARCH ARTICLE
10.1002/2016MS000699

Modeling the QBO—Improvements resulting from higher-model vertical resolution

Marvin A. Geller[1], Tiehan Zhou[2,3], D. Shindell[4], R. Ruedy[2,5], I. Aleinov[2,3], L. Nazarenko[2,3], N. L. Tausnev[2,5], M. Kelley[2,5], S. Sun[6], Y. Cheng[2,3], R. D. Field[2,7], and G. Faluvegi[2,3]

[1]School of Marine and Atmospheric Sciences, Stony Brook University, Stony Brook, New York, USA, [2]NASA Goddard Institute for Space Studies, New York, New York, USA, [3]Center for Climate Systems Research, Columbia University, New York, New York, USA, [4]Earth and Ocean Sciences, Nicholas School of the Environment, Duke University, Durham, North Carolina, USA, [5]Trinnovim LLC, New York, New York, USA, [6]NOAA/Earth System Research Laboratory, Boulder, Colorado, USA, [7]Department of Applied Physics and Applied Mathematics, Columbia University, New York, New York, USA

Abstract Using the NASA Goddard Institute for Space Studies (GISS) climate model, it is shown that with proper choice of the gravity wave momentum flux entering the stratosphere and relatively fine vertical layering of at least 500 m in the upper troposphere-lower stratosphere (UTLS), a realistic stratospheric quasi-biennial oscillation (QBO) is modeled with the proper period, amplitude, and structure down to tropopause levels. It is furthermore shown that the specified gravity wave momentum flux controls the QBO period whereas the width of the gravity wave momentum flux phase speed spectrum controls the QBO amplitude. Fine vertical layering is required for the proper downward extension to tropopause levels as this permits wave-mean flow interactions in the UTLS region to be resolved in the model. When vertical resolution is increased from 1000 to 500 m, the modeled QBO modulation of the tropical tropopause temperatures increasingly approach that from observations, and the "tape recorder" of stratospheric water vapor also approaches the observed. The transport characteristics of our GISS models are assessed using age-of-air and N_2O diagnostics, and it is shown that some of the deficiencies in model transport that have been noted in previous GISS models are greatly improved for all of our tested model vertical resolutions. More realistic tropical-extratropical transport isolation, commonly referred to as the "tropical pipe," results from the finer vertical model layering required to generate a realistic QBO.

Key Points:
- Fine vertical resolution is required for the simulated QBOs to properly extend to the tropical tropopause layer
- Finer vertical resolution leads to the better simulation of stratospheric transport
- Increasing vertical resolution improves the simulation of the atmospheric tape recorder

Correspondence to:
M. A. Geller,
marvin.geller@stonybrook.edu

Citation:
Geller, M. A., et al. (2016), Modeling the QBO—Improvements resulting from higher-model vertical resolution, *J. Adv. Model. Earth Syst.*, *8*, 1092–1105, doi:10.1002/2016MS000699.

Received 25 APR 2016
Accepted 7 JUN 2016
Accepted article online 9 JUN 2016
Published online 13 JUL 2016

1. Introduction

The quasi-biennial oscillation (QBO) is the dominant mode of variability in the equatorial lower and middle stratosphere [*Baldwin et al*., 2001]. There was a relatively short period of time between the discovery of the QBO by *Reed et al*. [1961] and *Veryard and Ebdon* [1961], and the development of the theory to explain it by *Wallace and Holton* [1968], *Lindzen and Holton* [1968], and *Holton and Lindzen* [1972]. Nevertheless, a long period ensued before the QBO was self-consistently modeled in an atmospheric general circulation model by *Takahashi* [1996]. The lack of a self-consistently generated QBO in such models was a problem in that the QBO is known to affect the extratropical climate in both the stratosphere [e.g., *Holton and Tan*, 1982] and the troposphere [e.g., *Marshall and Scaife*, 2009], and has also been suggested to be important in affecting the behavior of Atlantic hurricanes [e.g., *Gray*, 1984] and Pacific typhoons [e.g., *Ho et al*., 2009]. There has been a great deal of recent progress, so that now almost all state-of-the-art climate models have shown the capability to self-consistently model the QBO [e.g., *Scaife et al*., 2000; *Giorgetta et al*., 2006; *Hurwitz et al*., 2011; *Richter et al*. 2014; *Rind et al*., 2014].

This paper concerns our efforts at modeling the QBO at the NASA Goddard Institute for Space Studies (GISS) using model GISS-E2. We present a number of modeling results aimed at clarifying the role of parameterized small-scale gravity waves and resolved equatorial waves in determining the period, the downward extension, and the amplitude of the QBO. This paper expands on results of *Giorgetta et al*. [2006] in showing some of the ancillary benefits of properly modeling the wave-mean flow interactions that are necessary to produce a realistic QBO, namely an improved stratospheric H_2O tape recorder and desirable differences in the UTLS age-of-air. Age-of-air and N_2O transport diagnostics show a marked improvement over the earlier versions of GISS model that were used by *Shindell et al*. [2013]. These improvements in transport

show little dependence on model vertical resolution, but rather are associated with our gravity wave treatments.

2. Simplified Theory of the QBO

Plumb [1982] showed a schematic (reproduced in *Andrews et al*. [1987, p. 321]) in which two upward propagating atmospheric waves, one with a phase speed +c and another with a phase speed –c, could reproduce the essence of the QBO. The physics of this schematic is most aptly discussed using Eliassen and Palm's Theorem 1 [see *Eliassen and Palm*, 1961; also *Lindzen*, 1990],

$$\overline{p'w'} = -(u_0 - c)\rho_0 \overline{u'w'}, \tag{1}$$

where p is atmospheric pressure, w is vertical velocity, u is zonal velocity, c is the wave phase velocity, and ρ is atmospheric density. The subscripts $()_0$ denotes mean state variables, the superscript $()'$ denotes wave variables, and the overbar denotes averaging over wave phase. The expression $\overline{p'w'}$ is the wave upward energy flux, and $\rho_0\overline{u'w'}$ is the upward flux of gravity wave zonal momentum. Strictly speaking, "wave momentum flux" is a misnomer for the quantity relevant to wave-mean flow interaction, which should strictly be termed "pseudomomentum flux" [*Andrews and McIntyre*, 1978]; however, for our purposes, the distinction is not relevant, so we use the simpler term "momentum flux."

Equation (1) indicates that for an upward propagating wave ($\overline{p'w'} > 0$), the momentum flux ($\rho_0\overline{u'w'}$) is positive (i.e., westerly) if the wave phase speed is greater than the mean zonal flow (i.e., $u_0 - c < 0$). Thus, in this case, if the waves are being dissipated, the mean zonal flow will be accelerated toward the wave phase speed c. In the same manner, if the wave phase speed is less than the mean zonal flow ($u_0 - c > 0$) and there is dissipation, the mean zonal flow will be decelerated toward the phase speed c. If the mean zonal flow is westerly the wave with the positive phase speed +c will be preferentially absorbed, since $u_0 - c$ is small for this wave, accelerating the mean flow toward +c, and the mean zonal flow maximum will descend until the shears near the surface become so great that this westerly shear zone is destroyed by diffusive processes. In the meantime, the wave with negative phase speed freely propagates to higher altitudes, providing easterly winds at high levels that descend with time. In this manner, alternating descending westerly and easterly shear zones are produced. The shear zones will descend more quickly with increasing wave momentum fluxes, producing an oscillation with shorter period, and if greater phase speed waves are present, the descending westerlies and easterlies will have greater magnitude, producing a QBO with higher amplitude. Thus, in this very simple picture, the QBO period depends on the magnitude of the upward wave momentum fluxes, and the QBO amplitude depends on the wave phase speeds. Extensions of this simple two-wave picture of the QBO to include more waves and Brewer-Dobson tropical upwelling have been done by *Saravanan* [1990] and *Dunkerton* [1997], among others, and the GISS modeling presented in this paper includes all of these effects. Note that interactive chemistry also exerts influence on both the QBO period and the QBO amplitude [*Butchart et al*., 2003].

3. Brief Model Description

The basic model structure used in this paper is the GISS ModelE2, which was used in the Coupled Model Intercomparison Project's fifth phase (CMIP5) and has been described and compared to observations in *Schmidt et al*. [2014]. There are important differences, however. These differences are in the formulation of stratospheric gravity wave drag described in *Schmidt et al*. [2014, section 2.3]. In the CMIP5 version of ModelE2, formulations for orographically and deformation-forced gravity waves are used following the treatment of *Rind et al*. [1988]. Furthermore, a Rayleigh drag is used in the top four model layers (above about 1 hPa). The resulting mean zonal wind, shown in *Schmidt et al*. [2014, Figure 12] is too weak compared to observations during the DJF (December-January-February) season, and *Schmidt et al*. [2014] indicate that stratospheric variability in wind and temperature is also too weak.

We emphasize that in the results reported here, the basic dynamics and tropospheric physics structure of the GISS model are not changed. We use an identical model structure except for the following. The gravity wave and Rayleigh drags have been removed, and replaced with the *MacFarlane* [1987] orographic and *Alexander and Dunkerton* [1999] nonorographic gravity wave treatments, as was done in *Geller et al*. [2011]

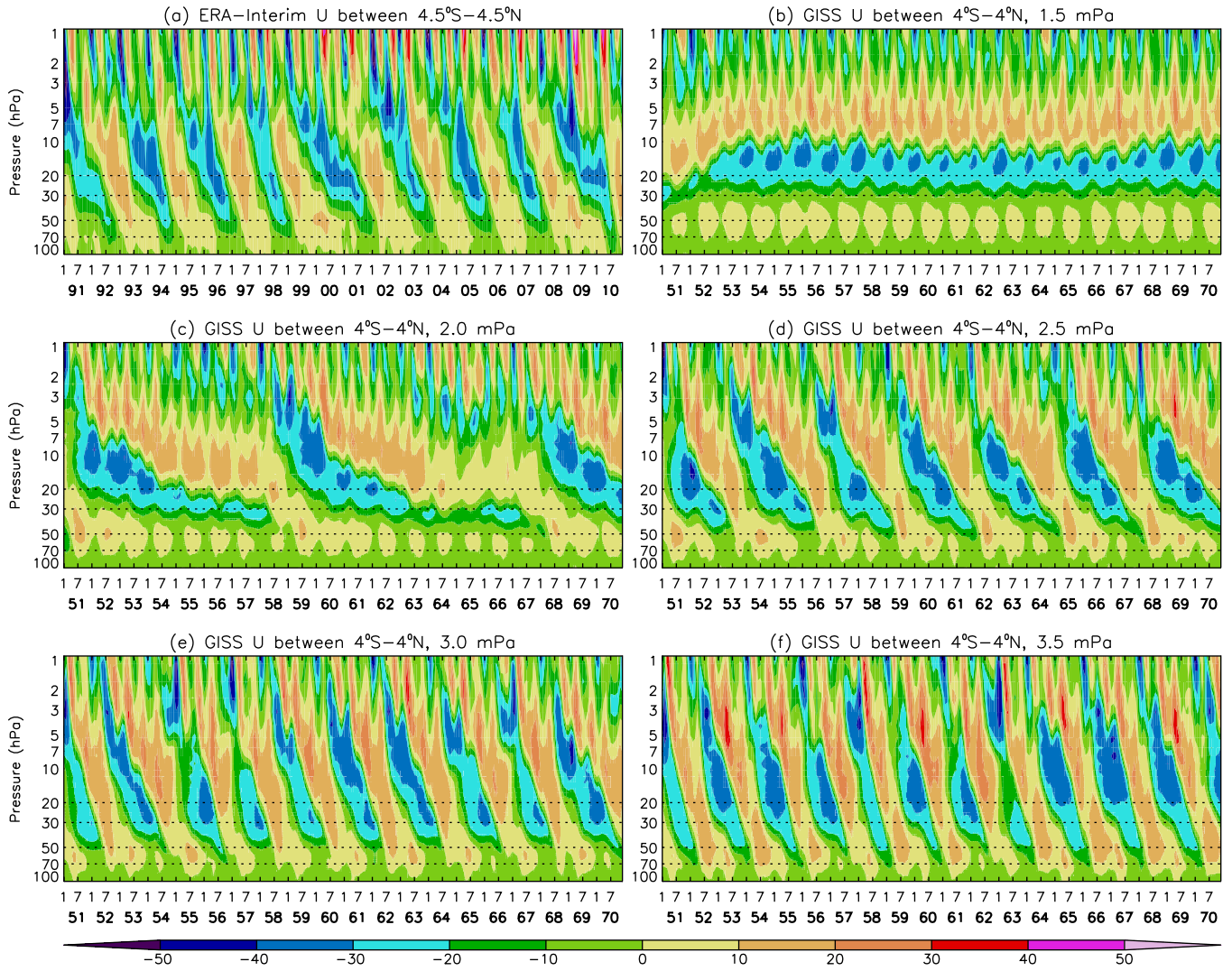

Figure 1. QBO mean zonal winds between 4°S and 4°N from (a) ERA Interim and modeled QBOs for gravity wave momentum flux forcings at 100 hPa having peak forcings of (b) 1.5 mPa, (c) 2.0 mPa, (d) 2.5 mPa, (e) 3.0 mPa, and (f) 3.5 mPa. In all cases, the B_2 gravity wave spectrum was used, zonally symmetric and centered on the equator, with a half width of 10° latitude, and a spectral spread of $c_w = 10$ m s^{-1}, and a 79-layer configuration was used. Color scale at the bottom indicates wind speed in m s^{-1}.

where a phase speed spectral shape B_2 [see *Gong et al*., 2008] with a spectral half-width of 10 m s^{-1} is nominally employed. Also, we vary the vertical layering in the stratosphere from the 40 layers used in *Schmidt et al*. [2014] in many cases. This will be further elaborated upon in subsequent sections.

4. Variations in Gravity Wave Momentum Fluxes

In section 2, we indicated that the simple two-wave model of the QBO, together with the implications of Eliassen and Palm's Theorem 1, suggests that increased gravity wave momentum fluxes should lead to faster descent of the zonal wind shear zones, and hence to shorter QBO periods.

Figures 1b–1f show the results of calculations of the model with vertical layering as depicted in Figure 3, where the only differences are in the specified nonorographic gravity wave momentum fluxes at 100 hPa while Figure 1a shows the QBO as represented in the ERA-Interim data assimilation. These simulations have been carried out in an Atmospheric Model Intercomparison Project (AMIP) style with repeated annual-cycle sea surface temperatures and sea-ice concentrations.

The mean zonal winds from the ERA-Interim reanalysis are shown between 4.5°S and 4.5°N between heights of 100 and 1 hPa for the 20 years 1991–2010. Note that ERA-Interim shows that approximately 8 1/2 QBO

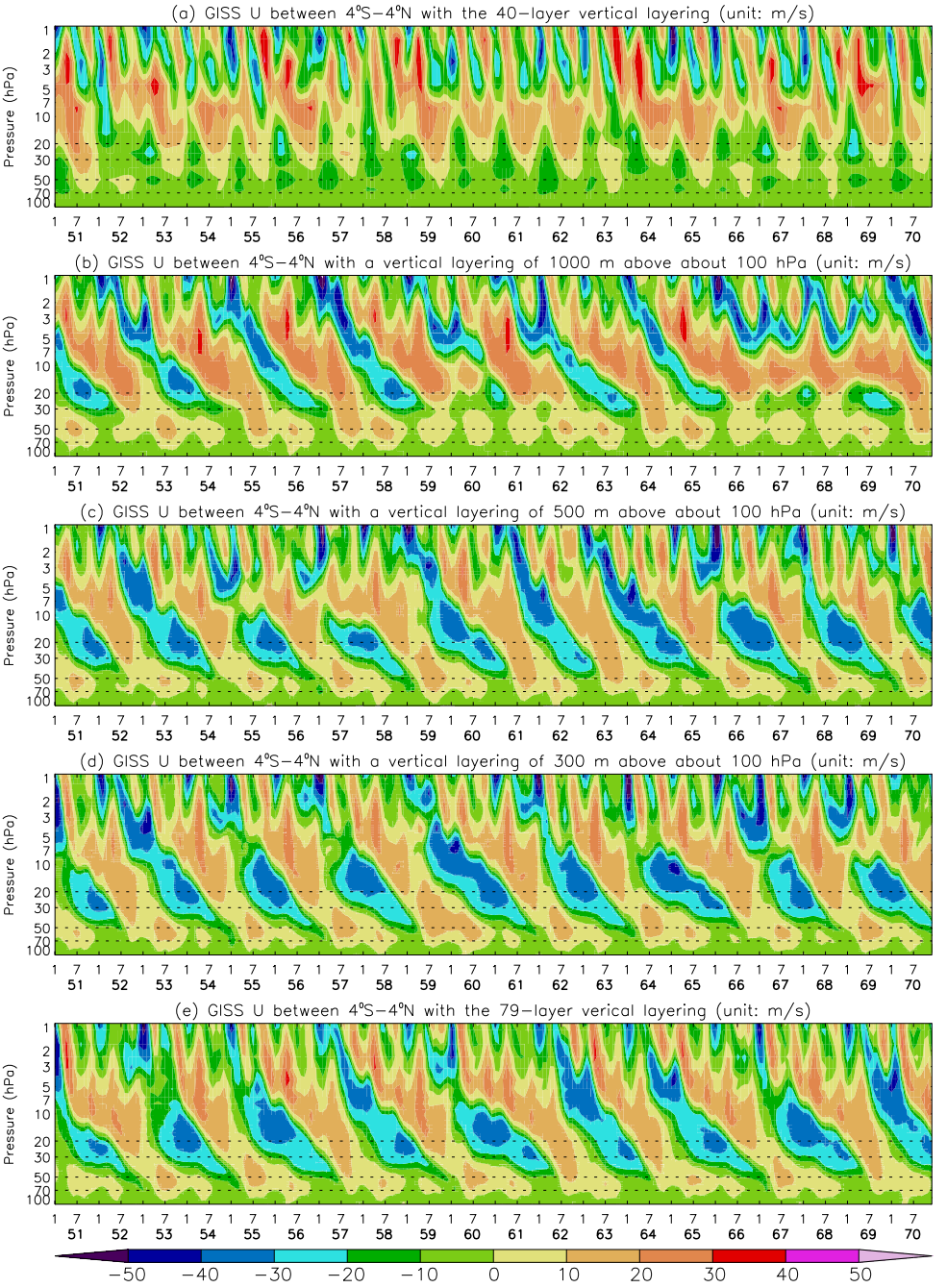

Figure 2. Modeled QBOs with different vertical layering. (a) The zonal mean zonal winds averaged between 4°S and 4°N with the 40-layer vertical layering of ModelE2. Similar to Figure 2a, (b–d) the results for a vertical layering of 1000, 500, and 300 m, respectively from about 100 to 5 hPa. Figure 2e uses the 79-layer layering shown in Figure 3. All the results in this figure use near-equatorial gravity wave phase speed source spectrum at 100 hPa described in the Figure 1 caption with a maximum gravity wave momentum flux of 2.9 hPa.

cycles occurred during this period, implying a QBO period averaging about 28 months. The model results in Figure 1b show that no coherent QBO resembling observations exists for the gravity wave momentum flux forcing of 1.5 mPa, which is consistent with the steady jets at low wave forcing demonstrated by *Yoden and Holton* [1988]. It also shows that the QBO-like oscillation for a gravity wave momentum flux forcing of 2.0 mPa has a period of about 8 years, while a forcing of 2.5 mPa gives a period of about 37 months, and a forcing of 3.0 mPa gives a period of about 25 months, and a forcing of 3.5 mPa gives a period of about 21 months. In fact, we find that the best fit to observed QBO periods is for a gravity wave momentum flux forcing of 2.9 mPa, as will be shown in the next section.

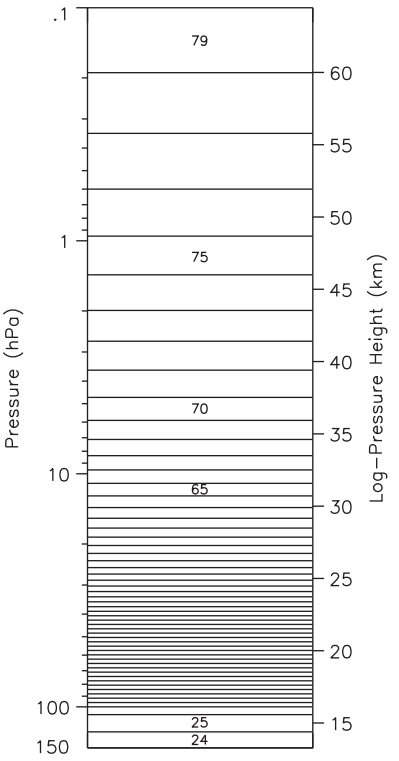

Figure 3. Vertical layering above the 150 hPa level for the 79-layer model configuration.

Thus, we find that the QBO period in our model depends on the specified nonorographic gravity wave fluxes even though resolved waves make a very significant contribution to the momentum forcing of the QBO, especially at lower levels [see *Scaife et al*., 2000; *Giorgetta et al*., 2006, for instance]. Others [e.g., *Giorgetta et al*., 2006; *Rind et al*., 2014] have also noted the sensitivity of the modeled QBO to the magnitude of the gravity wave momentum flux.

5. Influence of Vertical Resolution

Conventional wisdom is that a vertical resolution of less than 1 km is needed to properly model the QBO in a general circulation model [e.g., *Scaife et al*., 2000; *Giorgetta et al*., 2006]. We explore further the needed vertical resolution to properly model the QBO, due to our desire to explore what is needed to get a proper extension of the QBO into the lower stratosphere/upper troposphere region, since it is likely that a realistic downward extension of the QBO to the UTLS is needed to properly treat stratosphere-troposphere interactions involving the QBO.

Figure 2 shows modeled QBOs with a variety of vertical resolutions. Figure 2a shows the modeled QBO with the standard, 40-layer configuration used in ModelE2, where a gravity wave momentum flux of 2.9 mPa at the equator is used. Note that this vertical resolution is not sufficient to get a realistic QBO. Figure 2b used a 1000 m vertical resolution above about 100 hPa, and we see a rather realistic QBO, but this QBO wind variation is not penetrating to sufficiently low altitudes. This is most obvious when one compares the ERA-Interim QBO in Figures 1a–2b. The 1000 m vertical resolution has easterly QBO winds exceeding 10 m s^{-1} extending downward only slightly below 30 hPa, whereas ERA Interim has these easterlies extending downward below 50 hPa in all QBO cycles, and below 70 hPa in a few of the cycles. Also, the westerlies extend downward to about 100 hPa in ERA Interim, whereas they only extend a bit below 70 hPa in Figure 2b with the 1000 m vertical resolution. The 500 m vertical resolution results in Figure 2c exhibit greater downward extension of the westerlies than the 1000 m case, but still not as much as in the ERA Interim QBO results. There is greater downward penetration of the QBO easterlies with 500 m vertical resolution, but easterlies of about 10 m s^{-1} barely extend down to 50 hPa, except in a couple of cycles, and the QBO westerlies also do not extend as far downward as in ERA Interim. The 300 m vertical resolution results in Figure 2d are very similar to those in Figure 2c. Figure 2d indicates that the easterlies with speeds greater than 10 m s^{-1} extend downward to 50 hPa in all QBO cycles, and reach 70 hPa during one cycle, in approximate agreement with ERA Interim. The QBO westerlies extend almost to 100 hPa in all cycles, not quite as low as in ERA Interim. Finally, Figure 2e shows results for a 79-layer configuration that we have adopted as our nominal vertical resolution used to generate the results shown in Figure 1. It has 44 less layers than the model with 300 m vertical resolution throughout, but seems to give comparably good QBO results to the 300 m vertical resolution case. This 79-layer vertical resolution is shown in Figure 3 above 150 hPa. Below this level, the layering is identical to that shown in *Schmidt et al.* [2014, Figure 1]. It is interesting that the largest amplitude QBO is seen with the 1000 m vertical resolution. We believe that the reason for this is as follows. Note that the easterlies around 20 hPa are weakest in the 1000 m resolution case. This is because the deposited easterly momentum flux from wave breaking is being distributed over a deeper layer, resulting in weaker easterlies around 20 hPa. These weaker easterlies will cause less reflection of westerly propagating waves near the positive extreme of the gravity wave phase speed spectrum, so more westerly momentum flux is available to be deposited at higher levels.

In the preceding section, it has been shown that the specified gravity wave source momentum flux in the *Alexander and Dunkerton* [1999] parameterization is the controlling factor in the speed of the descent of the shear layers, and hence in QBO periods, but we have also seen that high vertical resolution is required for the QBO to descend to lower levels, as is observed. Our interpretation of these results is as follows. There

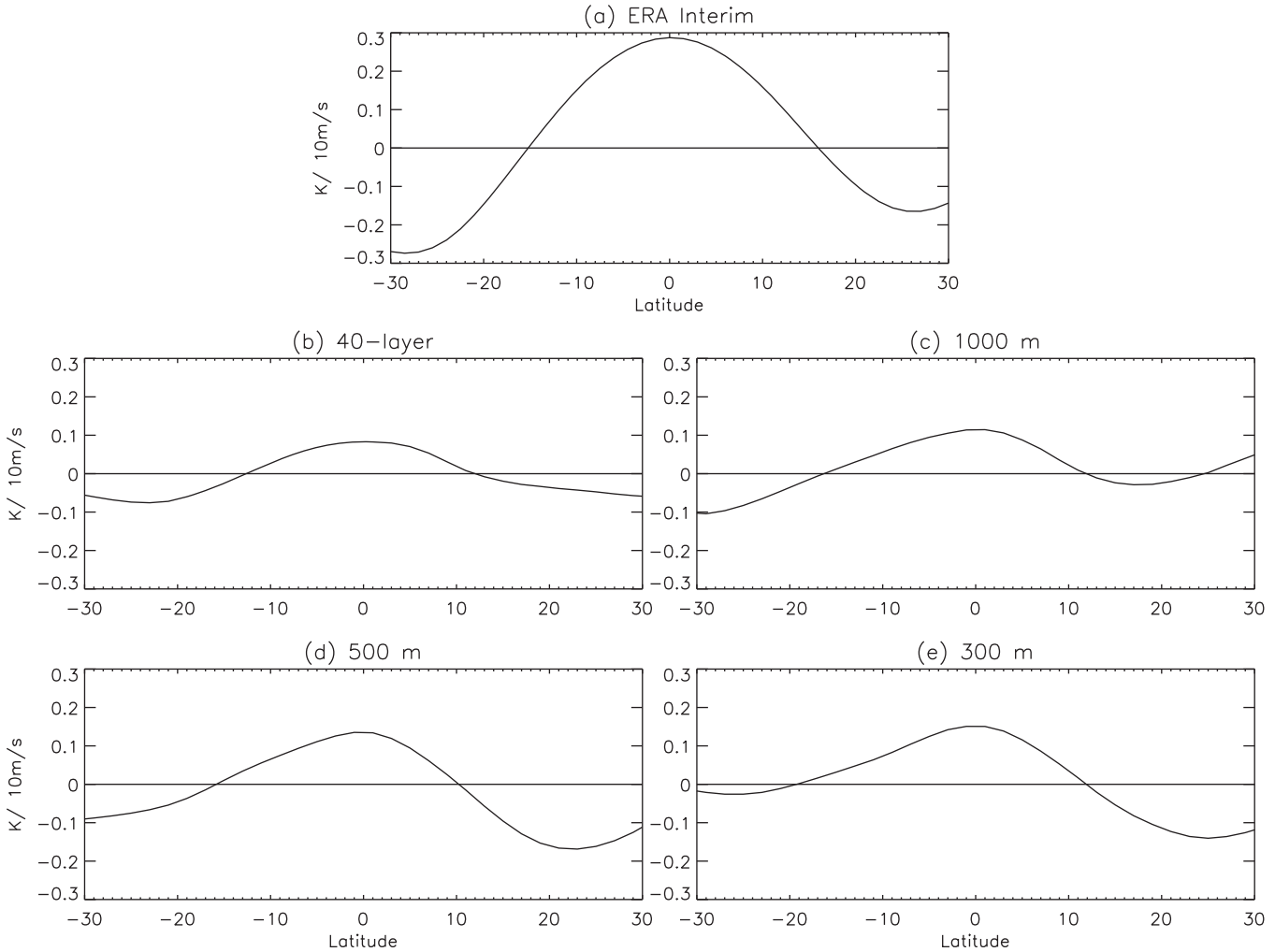

Figure 4. QBO modulations of the 100 hPa temperature from (a) the ERA Interim reanalysis; (b) the 40-layer GISS model; and the GISS model with vertical layering of (c) 1000 m, (d) 500 m, and (e) 300 m from 100 to 5 hPa pressure level. Note that the temperature modulation is shown per 10 m s^{-1} of the QBO at 50 hPa, and was derived in a similar manner to that in *Randel et al*. [2000] to derive their Figure 13.

must be sufficient small-scale gravity wave momentum flux in equatorial regions to develop a shear zone that descends through the upper stratosphere into the middle stratosphere. The descent rate of these shear zones is controlled by the magnitude of the gravity wave momentum flux from below. The large-scale waves resolved by the climate model then interact with the descending shear zones, and this propagates the QBO downward to the lower stratosphere/upper troposphere levels. Proper numerical resolution of these model-resolved wave-mean flow interactions requires sufficient vertical resolution. We find that a vertical resolution of about 500 m is required for the QBO to propagate toward tropopause altitudes, as observed. We expand on this in the following section.

6. QBO Modulation of Tropical Tropopause Temperatures

Using radiosonde data, *Reid and Gage* [1985] noted that there was an interannual variation of the tropical tropopause, which was induced by the QBO. This was followed up by later investigations by *Randel et al*. [2000], also using radiosonde data, and by *Zhou et al*. [2001], using ERA analyses. Realistic penetration of the QBO into the UTLS region is likely crucial for correctly modeling some of the QBO-induced stratosphere-troposphere interactions (e.g., QBO influences on tropical rainfall [see *Collimore et al*., 2003; *Liess and Geller*, 2012]). Figure 4 shows the QBO modulation of 100 hPa temperature (a proxy for tropopause temperature) in the GISS model with the various vertical layerings corresponding to what was shown in Figure 2. Note

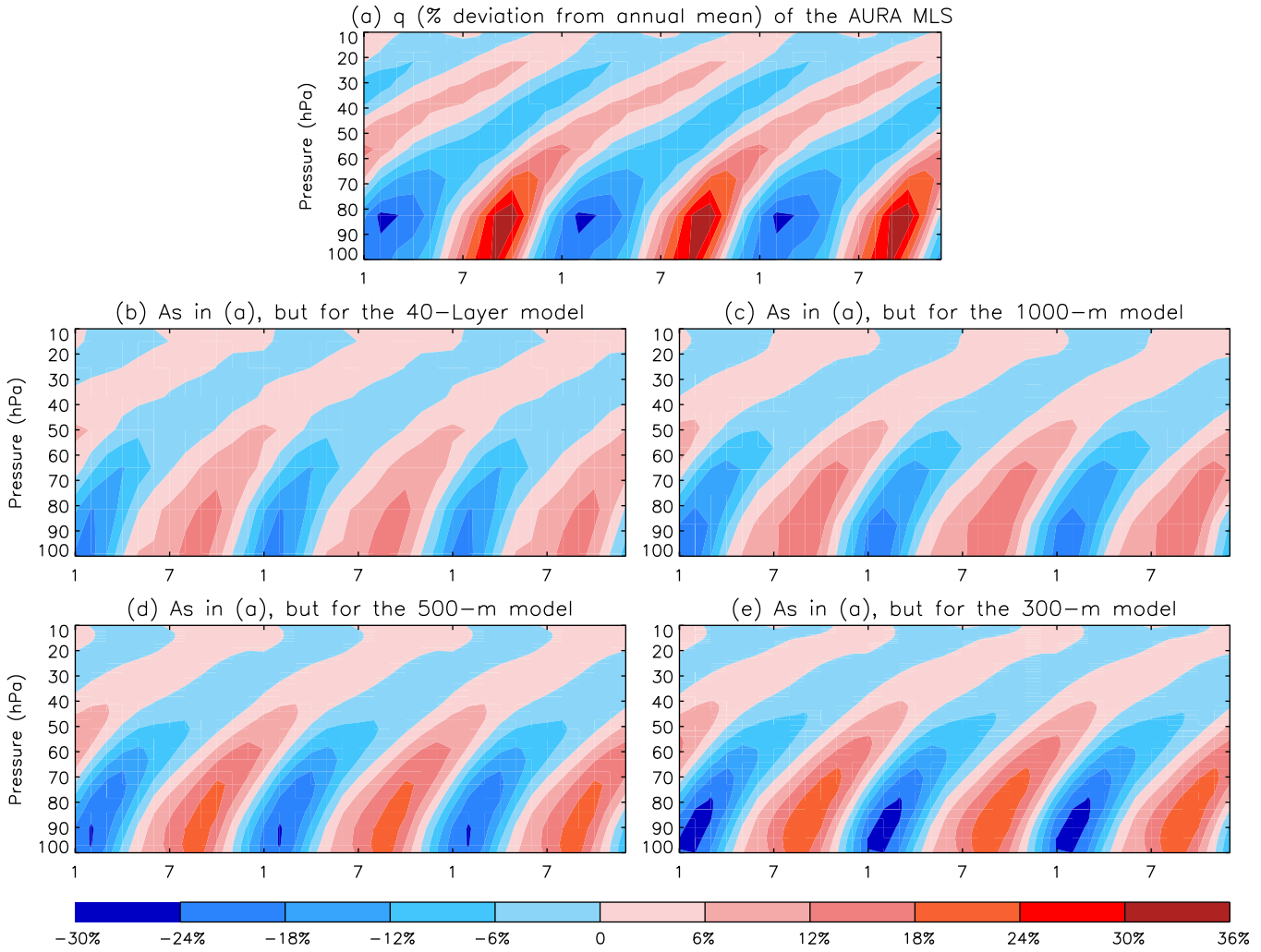

Figure 5. The percent deviation from the mean in specific humidity compared to the AURA MLS data in the tropical upper troposphere/lower stratosphere (12°S–12°N). Each plot depicts a climatology that is repeated 3 times to facilitate visualizing the tropical "tape-recorder" signal (a) from AURA MLS observations, (b) from 40-layer model, (c) from 1000 m model, (d) from 500 m model, and (e) from 300 m model. The ordinate is pressure in hPa. The abscissa indicates the calendar months, where the tick-mark of 1 indicates January and the tick-mark of 7 indicates July. The contour intervals are 6%.

that the total QBO modulation of the 100 hPa temperature derived from ERA Interim is a little less than 0.6 K, which compares well with what is shown in *Randel et al.*'s [2000, Figure 13]. This is to be compared to QBO modulations of about 0.15 K for the 40-layer GISS model; a little more than 0.2 K in the 1000 m layered GISS model; about 0.3 K in the 500 m layered GISS model; and similarly about 0.3 K in the 300 m layered GISS model. Surprisingly, we do find a significant QBO modulation in the 100 hPa temperatures in the 40-layer model even though there is little evidence of the QBO wind modulations extending down to that level in Figure 2b. The apparent lack of the QBO in Figure 2b is just due to our chosen contour interval for Figure 2. Clearly though, the QBO 100 hPa temperature modulations increase as the vertical layering is increased. In the 40-layer model, the QBO temperature amplitude is about 0.15 K/10 m s^{-1}, whereas with 1000 m layering, it is about 0.2 K/10 m s^{-1}; and with 500 m layering, it is about 0.3 K/10 m s^{-1}; and with 300 m layering, it is slightly more than with the 500 m layering. It should be noted that we would expect QBO model modulations of tropopause temperatures to be less than are seen from radiosonde measurements, since radiosonde vertical resolution is much greater than model layering.

7. The "Tape-Recorder" Signal of Stratospheric Water Vapor

The "tape-recorder" signal in stratospheric water vapor [*Mote et al.*, 1996] is a good indicator of the annual modulation of tropical tropopause temperatures [e.g., *Zhou et al.*, 2004], of tropical upwelling, as well as of

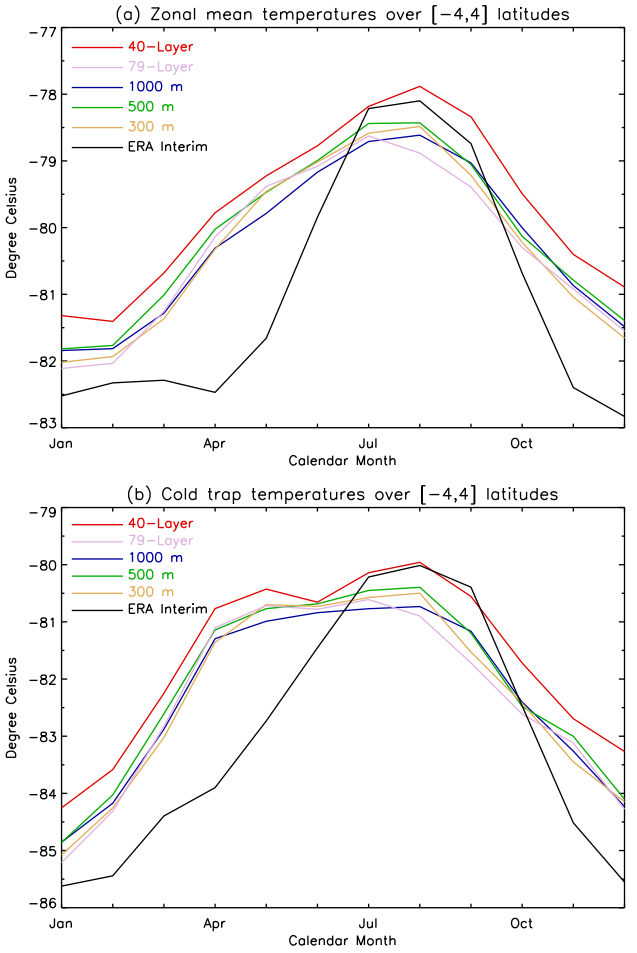

Figure 6. (top) Climatological annual cycle of the zonally averaged 100 hPa temperatures, averaged from 4°S to 4°N, from ERA Interim (black) over the 1979–2014 period and from the GISS model with the various layerings (with colors as indicated). (bottom) Same, but for the temperature values at the longitude where the 100 hPa temperatures averaged from 4°S to 4°N are minimum.

the degree of tropical/extratropical isolation. Figure 5 shows the "tape-recorder" signal from observations, as well as for the various GISS model layerings. The dryness signal at about 100 hPa is due to the rising air parcels having been dehydrated by passing through the very cold tropical tropopause dehydration regions at the time of Northern Hemisphere winter [see *Holton and Gettelman*, 2001; *Zhou et al.*, 2004] while the moist signal is due to warmer tropical tropopause temperatures existing at the time of Northern Hemisphere summer and direct convective insertion of moisture into the stratosphere. The slope of the dry and moist signals is a reflection of the tropical upwelling. Finally, the vertical extent of the "tape-recorder" signal is indicative of the isolation between the tropics and extratropics.

The amplitude of the signal at 80–90 hPa is about 54% in the Aura MLS v3.3 H_2O [*Livesey et al.*, 2011, and references therein] over the 2005–2012 period, whereas it is only about 30% in the 40-layer model, about 30% with the 1000 m layering, and about 42% with both 500 and 300 m layering, so all the model layerings give too small a "tape-recorder" signal. To see why this is so, Figure 6 shows the average annual cycle of both the zonally averaged 100 hPa temperature from the ERA Interim reanalysis and of the minimum 100 hPa temperatures along the equator, together with the same quantities for the various GISS model layerings discussed in this paper. Note first that the minimum temperatures are a few degrees colder than the zonally averaged temperatures, reflecting the temperatures at the "cold trap" where air parcels passing through are dehydrated to the values where they enter the stratosphere in the rising branch of the Brewer-Dobson circulation, which, of course, is to be expected. Apparently, Figure 6 indicates that the inadequate seasonal cycle of simulated temperatures in the tropical tropopause layer results in the weaker simulated "tape-recorder" signals shown in Figure 5. Note also that there is a much more marked asymmetry in the cold versus warm months in ERA Interim than in any of the above mentioned GISS models. For instance, looking at the zonally averaged temperatures, the annual mean temperature from ERA Interim is about −81.3°C so that during the coldest month (December) when the temperature is −82.8°C, the negative temperature difference from the annual mean is about −1.5°C, while during the warmest month (August) when the temperature is −78.1°C, the corresponding positive temperature difference is +4.2°C. This is very different from the behavior of the modeled temperatures, where, taking the green curve (500 m layering) as an example, the annual mean temperature is about −80.1°C, so that during January and February (the coldest months) when the temperature is about −81.8°C, the temperature is colder by about −1.7°C, whereas during the warmest months, July and August when the temperature is about −78.5°C, the temperatures are warmer by about 2.3°C. Taking into account the nonlinear Clausius-Clapeyron equation, this likely accounts for most of the moister anomalies (in percentage terms) in the AURA MLS observations in Figure 5 relative to the models. The slope of the "tape-recorder" signal in

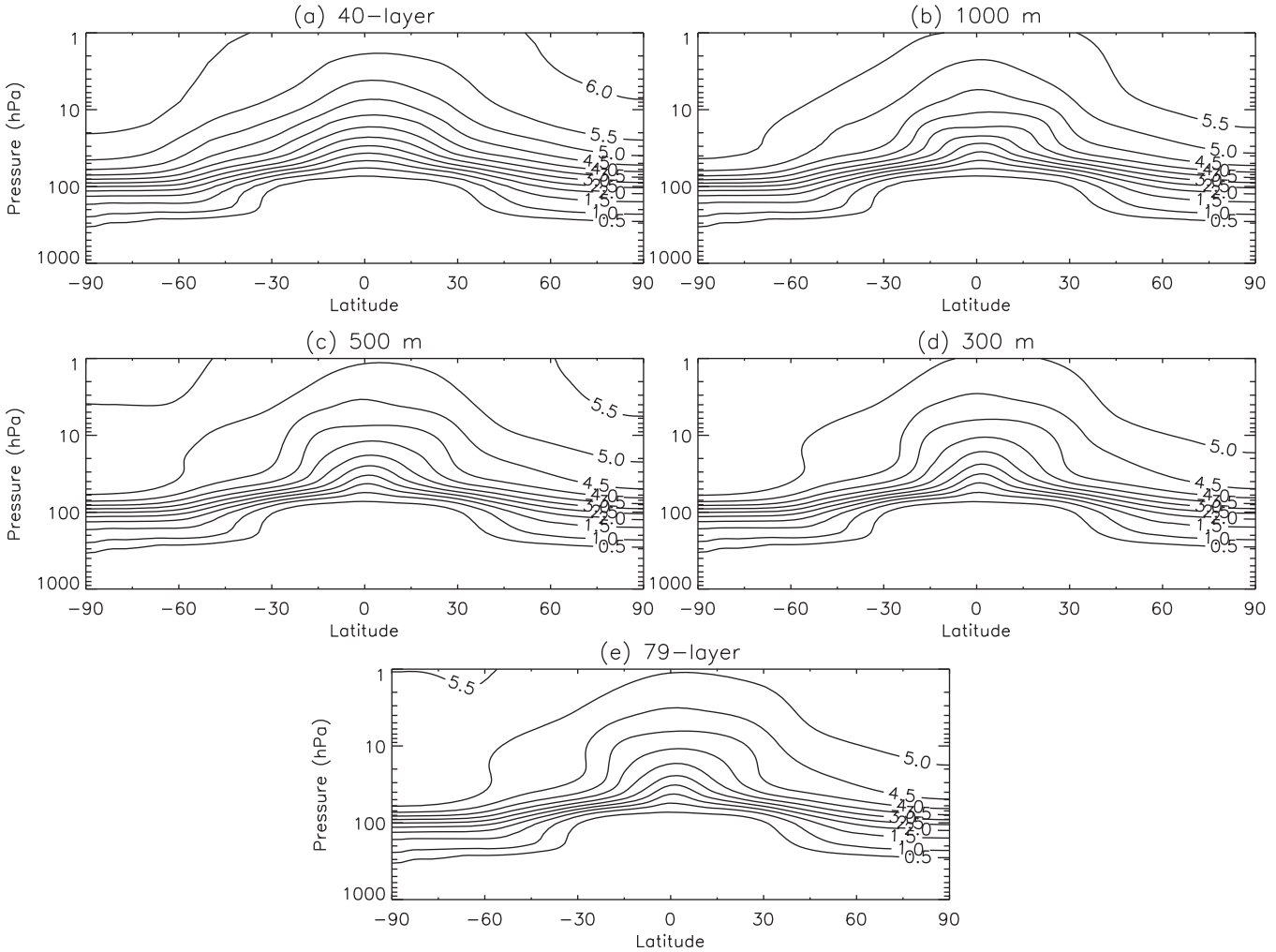

Figure 7. Twenty year averaged age-of-air from the (top left) 40-layer model, (top right) 1000 m layering, (middle left) 500 m layering, (middle right) 300 m layering, and (bottom) the 79-layer model. Positive latitudes are for the Northern Hemisphere, pressure altitudes are in hPa, and the contour intervals are 0.5 year.

Figure 5 is a reflection of the moisture anomaly signal being transported upward by the tropical upwelling velocity. Note that the slope seems to increase with increased vertical resolution. For instance, focusing on the first positive moisture anomaly cycle, one sees that the zero line in the observations seems to start in November at 100 hPa and reach 30 hPa in November of the following year, implying a lag of about 12 months between those two altitudes. The similar lag time for the 40-layer model is about 10 months; about 9 months with 1000 m layering; about 10 months with 500 m layering; and about 11 months with 300 m layering. Thus, this slope of the tape-recorder signal seems to approach observed values for finer vertical resolutions. This is likely due to the changes in the tropical upwelling vertical profile for changing vertical resolution [e.g., see *Giorgetta et al*., 2006, Figure 11] and the improved numerical accuracy of vertical advection term [*Hardiman et al*., 2015] associated with higher vertical resolution.

The vertical penetration of the moisture signals is an indication of the better simulated horizontal mixing between the tropics and the extratropics, since such mixing tends to dilute the strength of the signal. Noting that the dryness signal has comparable amplitude at 100 hPa to the observations and in all the different models, we look into the fraction by which the dryness signal diminishes from its minimum just above the tropopause to 50 hPa altitude. In the observations, the maximum dryness is about 24% and at 50 hPa it has decreased to about 9%. Thus, the dryness signal is diminished by about a factor of 0.38 in the observations. The analogous diminishing factor in the 40-layer model is about 0.2; while with 1000 m layering, it is also about 0.2; and with 500 m layering, it is about the same; and with 300 m layering, it is about 0.3. Thus, there

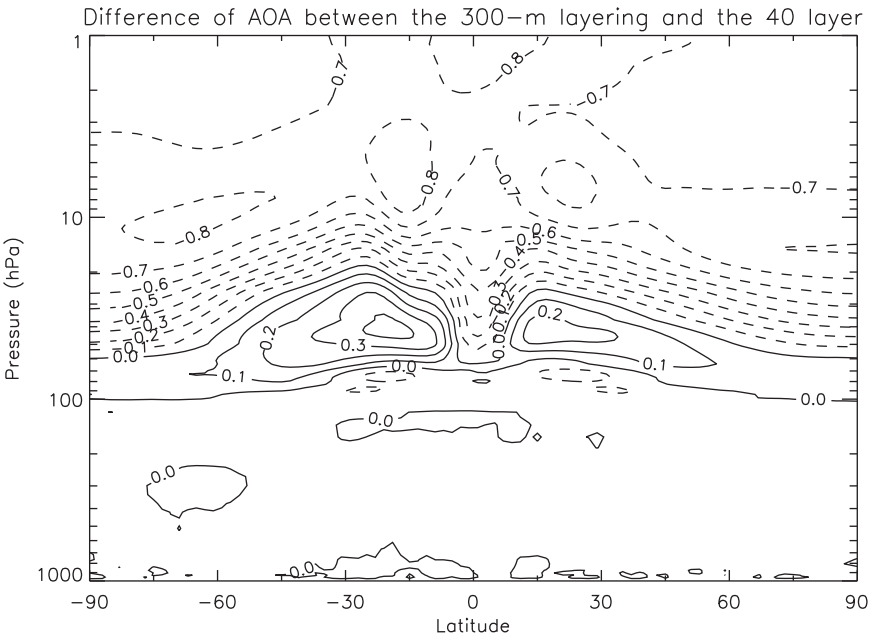

Figure 8. Difference in ages-of-air between the 300 m and the 40-layer GISS models.

seems to be less mixing between the tropics and extratropics with finer vertical resolution. We will explore this point further in the next section.

8. Age-Of-Air

Figure 7 shows the age-of-air for the differently layered models that we have explored so far in this paper. It is obvious visually in Figure 7 is that there is more tropical/extratropical isolation with narrowing vertical layering. This is obvious from the greater compression of the subtropical age-of-air contours with finer vertical layering. This reflects more of a "tropical pipe" [e.g., *Plumb*, 1996] in models with finer vertical layering.

In Figure 7, the age-of-air contours generally indicate shorter ages-of-air in the tropics but longer ages-of-air in the lower stratosphere in the subtropics to high latitudes. For instance, in the 40-level model, the age-of-air at 1 hPa at the equator is between 5.5 and 6.0 years, but with 300 m layering, the corresponding age-of-air is between 4.5 and 5.0 years, almost a full year shorter than in the 40-layer model.

These differences are more obvious in Figure 8, which shows the differences in age-of-air between the model with 300 m layering and the 40-layer model. Note that over the equator, the ages-of-air in the 300-layer model are shorter by about 0.1 years at low altitudes and shorter by about 0.8 years at high altitudes, but the ages-of-air are longer by about 0.4 years in the southern subtropics in the lowest stratosphere and longer by about 0.2 years in the northern subtropics. Thus, there is more isolation between the deep tropics and the subtropics with 300 m vertical layering than in the 40-layer model in the lower stratosphere.

It is well established that age-of-air contours approximately coincide with mixing ratio contours of long-lived tracers [e.g., *Mahlman*, 1985; *Yudin et al*., 2000], and that the slope of these contours is made steeper by the diabatic circulation, with diffusive effects acting to lessen the steepness. Thus, the results shown here suggest that increased vertical resolution in the GISS model have acted to intensify the diabatic circulation and decrease the diffusion between the tropics and extratropics.

This is seen in our annually averaged modeled N_2O, which is shown in Figure 9 for different vertical resolutions. Looking at the shape of the 200 ppb contour, we see more of a "high-hat" shape in the higher vertical resolution models, consistent with observations, while the 40-layer model contour shape has more of a smooth Gaussian appearance. Thus, the higher-resolution models show greater tropical-extratropical isolation, consistent with observations of N_2O.

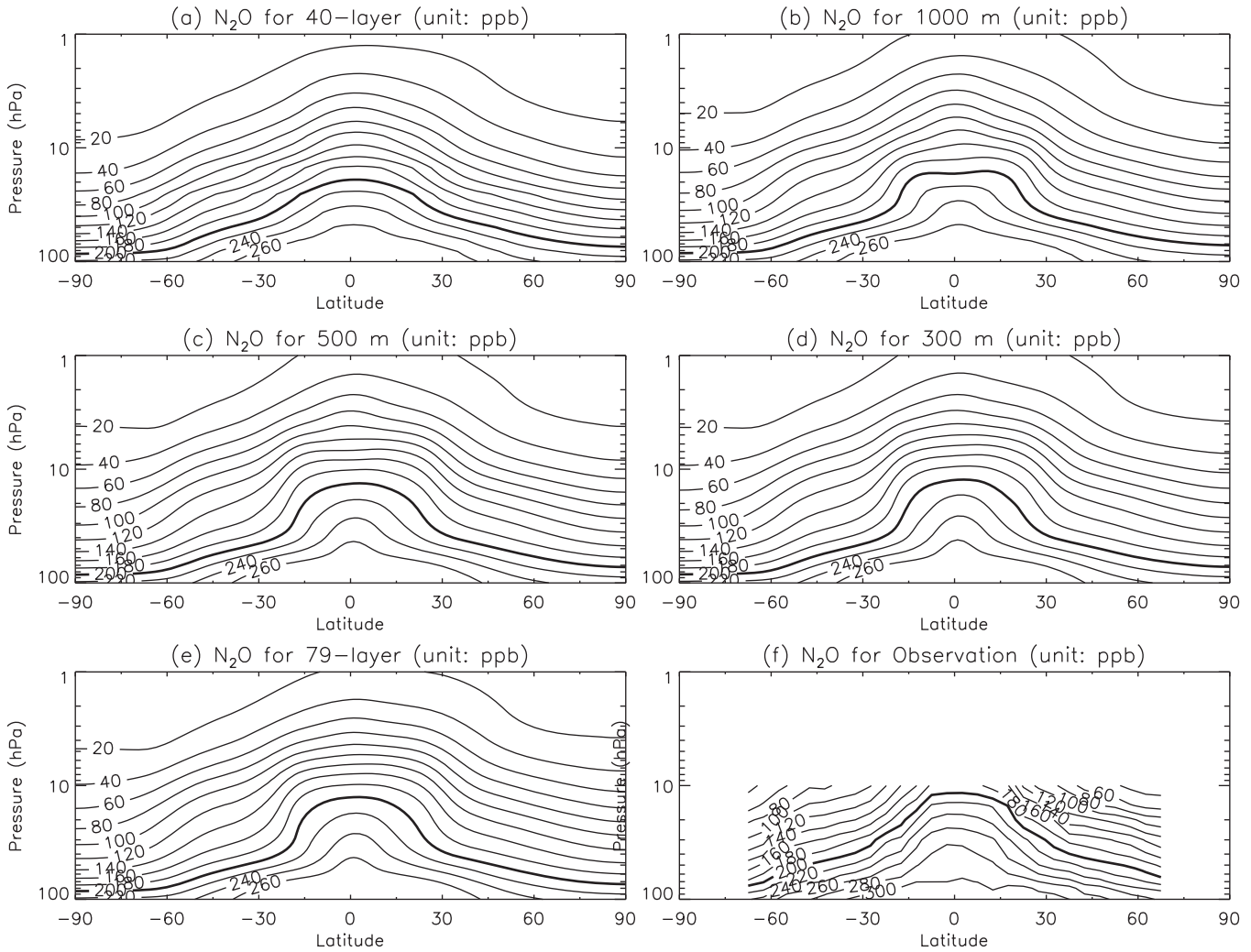

Figure 9. Annually averaged N_2O mixing ratios in ppb from (a) the 40-layer model, (b) the 1000 m layered model, (c) the 500 m layered model, (d) the 300 m layered model, (e) our 79-layer model, and (f) from ACE observations. Model results are averages for a 10 year run. Note that the N_2O observations were only available for the latitudes and pressure altitudes shown.

9. Assessment of Stratospheric Transport

Shindell et al. [2013] used observations of N_2O from the Atmospheric Chemistry Experiment (ACE) onboard SCISAT-1 during 2004–2009 and age-of-air derived from CO_2 and SF_6 balloon data, as described in *Strahan et al.* [2011] and *Andrews et al.* [2001] to diagnose stratospheric transport deficiencies in the GISS CMIP5 model. *Shindell et al.* [2013, Figure 7] indicated that when the near-global age-of-air was plotted against the near-global N_2O mixing ratios, the age-of-air was systematically too low. A similar plot in the tropics showed better agreement. In diagnosing the reasons behind this disagreement, *Shindell et al.* [2013] created plots similar to those in *Strahan et al.* [2011]. *Shindell et al.* [2013] plotted the model minus observations of tropical age-of-air versus pressure altitude and found that air was too young in the model's tropical lower stratosphere [see *Strahan et al.*, 2011]. *Shindell et al.* [2013] also examined the extratropical minus the tropical age-of-air gradient as a function of pressure altitude, and they found the model gradient to be systematically less than the values derived from observations, indicating too fast a stratospheric advective circulation (again according to *Strahan et al.* [2011]). Finally, *Shindell et al.* [2013] plotted the model minus the observed tropical N_2O as a function of pressure altitude, and they found the model values higher than those observed, indicating too little mixing between the tropics and midlatitudes, so the tropical air was too young [see *Strahan et al.*, 2011]. We repeated these calculations for all model vertical resolutions, and we found that there was little dependence of these results on vertical resolution, so in Figure 10, we only show results from our 40-layer model in the same format of *Shindell et al.* [2013, Figure 7].

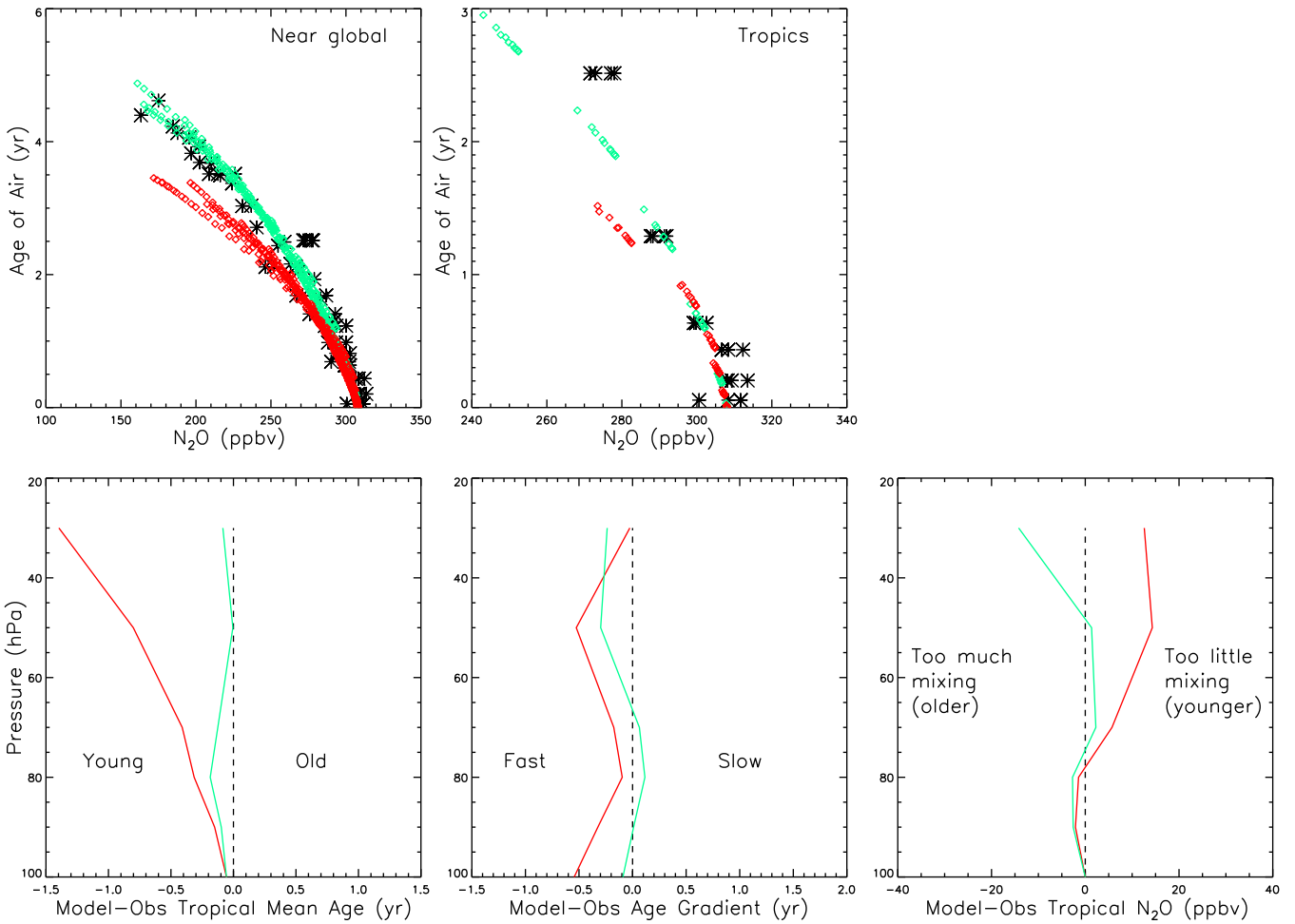

Figure 10. (top left) Scatterplot of near-global age-of-air versus N_2O mixing ratios, stars being observations, the red diamonds from the CMIP5 version of E2 driven by the MERRA reanalysis, and the green diamonds from the 40-layer GISS model run described in this study. (top right) Same as top-left except for the tropics. (bottom left) Model minus Observations for tropical age-of-air versus pressure-altitude. (bottom middle) Model minus Observed midlatitude-tropical age-of-air gradient as a function of pressure altitude. (bottom right) Model minus Observed tropical N_2O mixing ratio as a function of pressure altitude. Note that the yellow uncertainty shaded regions in *Strahan et al.* [2011] are not in this Figure 10.

Note that Figure 10 shows much better consistency between the model transport diagnostics and the observations than was the case with the GISS CMIP5 model in *Shindell et al.* [2013]. As indicated previously, plots similar to Figure 10 for the various vertical resolutions looked very similar, and the only substantial differences between our 40-layer GISS model and the CMIP5 GISS model was in the gravity wave treatment, indicating that it was that difference that accounted for the transport improvements.

10. Discussion

Earlier works by *Scaife et al.* [2000], *Giorgetta et al.* [2006], among others, and recent works by *Rind et al.* [2014] and *Richter et al.* [2014] have already established the important roles that parameterization of subgrid-scale gravity wave parameterizations and vertical resolution play in modeling a realistic QBO in a self-consistent manner, and the points brought up in the earlier sections of this paper are either explicitly or implicitly contained in those works, but we think it important to stress a few points. One is that sufficient gravity wave momentum flux is required to model the QBO in a self-consistent manner. Another point is that the magnitude of the subgrid-scale gravity wave momentum flux essentially determines the QBO period. Sufficient vertical resolution is then required to have this QBO penetrate to lower levels, as observed. This implies that success in simulating a realistic QBO in a climate model starts with establishing the subgrid-scale gravity wave momentum flux inducing wind shears that propagate down from the upper stratosphere. This takes place with even rather coarse vertical resolution. Finer vertical resolution is then

required for the model-resolved waves to interact with these downwardly propagating shears so that they continue down toward tropopause levels. Thus, a sort of "hand-off" between the gravity wave produced wind shears takes place in the middle stratosphere to the resolved waves for the QBO's further downward progression.

The magnitude of the QBO is determined by the width of the phase speed spectrum of gravity waves; that is to say, having sufficient gravity wave momentum flux at the higher phase speeds plays the most important role in determining the amplitude of the QBO [*Geller et al*., 2016]. Even with rather coarse vertical resolution, there is some QBO modulation of tropical tropopause temperatures, but for this QBO modulation of tropopause temperatures to approach the observed QBO modulation of those temperatures seems to require a vertical layering on the order of 500 m in our model.

There are three factors involved in obtaining a realistic annual "tape-recorder" signal. One is getting a realistic annual modulation of the tropical tropopause temperatures, and this seems to require good vertical resolution, on the order of 500 m or less. Another is obtaining realistic tropical upwelling velocities. This upwelling velocity from the models with higher vertical resolutions is seen to be faster in the lowest stratosphere, up to about 70 hPa, with an even faster upwelling velocity above. Another factor is the degree of isolation between the lower stratosphere tropics and extratropics. This isolation, often referred to as the "tropical pipe," becomes more realistic as vertical resolution is increased. This isolation is seen more clearly when one examines the "age-of-air" in models with different vertical resolutions. Note that many dynamical, radiative, and microphysical processes exert influence on the "tape-recorder" signal [*Hardiman et al*., 2015], and further discussion of this is beyond the scope of this paper.

Increasing the vertical resolution in the GISS model seems to lead to both an increased diabatic circulation and to sharper meridional gradients in the "age-of-air" between the tropics and extratropics. This dependence of the "age-of-air" on vertical resolution seems to result from better resolution of the resolved wave-mean flow interactions that also is responsible for the more realistic downward penetration of the QBO toward tropopause levels. We believe that this increased isolation between the tropics and extratropics is a result of better resolution of mixing in what was called the "surf zone" by *McIntyre and Palmer* [1984], but this deserves more investigation.

While our modeling of the annual "tape recorder" in stratospheric water vapor with relatively fine vertical resolution looks realistic in many respects, closer inspection shows that we do not obtain the observed amplitude of the moist signal just above tropopause levels. We have traced this deficiency to the fact that our modeled annual modulation in tropical tropopause temperatures is not in close agreement with that observed. This is likely due to our modeled cycle in extratropical planetary waves being different from the observed.

Giorgetta et al. [2006] have shown that the enhanced vertical resolution which enabled successful modeling of the QBO also led to other model improvements, and one of the purposes of this paper is to enlarge on that point. That is to say, the improved modeling of the wave-mean flow interactions that are involved in giving rise to the QBO also give rise to other model improvements. Still more research is needed to explore the beneficial effects of fine vertical resolution in troposphere-stratosphere climate models so that optimal combinations of horizontal and vertical resolutions can be employed.

Finally, we compared the stratospheric transport diagnostics for the CMIP5 version of the GISS model used by *Shindell et al*. [2013] with those for the version described in this paper. Our results indicated much better agreement between the simulated transport and that implied by observations. This was true for all our model vertical resolutions, so we conclude these improvements must be due to the differences in our gravity wave treatments from those used in the GISS CMIP5 model. We emphasize though that vertical resolution does seem to have a large influence on both tropical upwelling and mixing between the tropics and the extratropics, with the results from the higher vertical resolution models being in better agreement with observations.

Acknowledgments
This work was supported by the NASA Modeling, Analysis and Prediction Program and the NASA High-End Computing (HEC) Program through the NASA Center for Climate Simulation (NCCS) at Goddard Space Flight Center. Data from these runs are available from Tiehan Zhou (tz2131@columbia.edu). We thank Jae N. Lee for kindly providing the AURA MLS water vapor data. The authors acknowledge the two anonymous reviewers for their helpful comments, which led to an improved paper.

References

Alexander, M. J., and T. J. Dunkerton (1999), A spectral parameterization of mean-flow forcing due to breaking gravity waves, *J. Atmos. Sci.*, *56*, 4167–4182.

Andrews, A., et al. (2001), Mean ages of stratospheric air derived from in situ observations of CO_2, CH_4, and N_2O, *J. Geophys. Res.*, *106*, 32,295–32,314, doi:10.1029/2001JD000465.

Andrews, D. G., and M. E. McIntyre (1978), On wave-action and its relatives, *J. Fluid Mech.*, *89*, part 4, 647–664.

Andrews, D. G., J. R. Holton, and C. B. Leovy (1987), *Middle Atmosphere Dynamics*, 489 pp., Academic Press, Orlando, Fla.

Baldwin, M. P., et al. (2001), The quasi-biennial oscillation, *Rev. Geophys.*, *39*, 179–229, doi:10.1029/1999RG000073.

Butchart, N., A. A. Scaife, J. Austin, S. H. E. Hare, and J. R. Knight (2003), Quasi-biennial oscillation in ozone in a coupled chemistry-climate model, *J. Geophys. Res.*, *108*(D15), 4486, doi:10.1029/2002JD003004.
Collimore, C. C., D. W. Martin, M. H. Hitchman, A. Huesmann, and D. E. Waliser (2003), On The Relationship between the QBO and tropical deep convection, *J. Clim.*, *16*, 2552–2568.
Dunkerton, T. J. (1997), The role of gravity waves in the quasi-biennial oscillation, *J. Geophys. Res.*, *102*, 26,053–26,076.
Eliassen, A. N., and E. Palm (1961), On the transfer of energy in stationary mountain wave, *Geofis. Publ.*, *22*, 1–23.
Geller, M. A., T. Zhou, R. Ruedy, I. Aleinov, L. Nazarenko, N. L. Tausnev, S. Sun, M. Kelley, and Y. Cheng (2011), New gravity wave treatments for GISS climate models, *J. Clim.*, *24*, 3989–4002, doi:10.1175/2011JCLI4013.1.
Geller, M. A., T. Zhou, and W. Yuan (2016), The QBO, gravity waves forced by tropical convection, and ENSO, *J. Geophys. Res.*, in press.
Giorgetta, M. A., E. Manzini, E. Roeckner, M. Esch, and L. Bengtsson (2006), Climatology and forcing of the quasi-biennial oscillation in the MAECAM5 model, *J. Clim.*, *19*, 3882–3901, doi:10.1175/JCLI3830.1.
Gong, J., M. A. Geller, and L. Wang (2008), Source spectra information derived from U.S. high-resolution radiosonde data, *J. Geophys. Res.*, *113*, D10106, doi:10.1029/2007JD009252.
Gray, W. M. (1984), Atlantic seasonal hurricane frequency, part I, El Niño and 30 mb quasi-biennial oscillation influences, *Mon. Weather Rev.*, *112*, 1649–1668.
Hardiman, S. C., et al. (2015), Processes controlling tropical tropopause temperature and stratospheric water vapor in climate models, *J. Clim.*, *28*, 6516–6535.
Ho, C.-H., H.-S. Kim, J.-H. Jeong, and S.-W. Son (2009), Influence of stratospheric quasi-biennial oscillation on tropical cyclone tracks in the western North Pacific, *Geophys. Res. Lett.*, *36*, L06702, doi:10.1029/2009GL037163.
Holton, J. R., and A. Gettelman (2001), Horizontal transport and the dehydration of the stratosphere, *Geophys. Res. Lett.*, *28*, 2799–2802.
Holton, J. R., and R. S. Lindzen (1972), An updated theory for the quasi-biennial cycle of the tropical stratosphere, *J. Atmos. Sci.*, *29*, 1076–1080.
Holton, J. R., and H.-C. Tan (1982), The quasi-biennial oscillation in the Northern Hemisphere lower stratosphere, *J. Meteorol. Soc. Jpn.*, *60*, 140–148.
Hurwitz, M. M., P. Braesicke, and J. A. Pyle (2011), Sensitivity of the mid-winter Arctic stratosphere to QBO width in a simplified chemistry–climate model, *Atmos. Sci. Lett.*, *12*, 268–272, doi:10.1002/asl.330.
Liess, S., and M. A. Geller (2012), On the relationship between QBO and distribution of tropical deep convection, *J. Geophys. Res.*, *117*, D03108, doi:10.1029/2011JD016317.
Lindzen, R. S. (1990), *Dynamics in Atmospheric Physics*, 310 pp., Cambridge Univ. Press, N. Y.
Lindzen, R. S., and J. R. Holton (1968), A theory of the quasi-biennial oscillation, *J. Atmos. Sci.*, *25*, 1095–1107.
Livesey, N. J., et al. (2011), Earth Observing System (EOS) Aura Microwave Limb Sounder (MLS) version 3.3 level 2 data quality and description document, Version 3.3x-1.0, *JPL Tech. Rep. JPL-D-33509*, 162 pp., Jet Propul. Lab., Calif. Inst. of Technol., Pasadena. [Available at http://mls.jpl.nasa.gov/data/v3-3_data_quality_document.pdf.]
Mahlman, J. D. (1985), Mechanistic interpretation of stratospheric tracer transport, *Adv. Geophys.*, *28A*, 301–323.
Marshall, A. G., and A. A. Scaife (2009), Impact of the QBO on surface winter climate, *J. Geophys. Res.*, *114*, D18110, doi:10.1029/2009JD011737.
McFarlane, N. A. (1987), The effect of orographically excited gravity wave drag on the general circulation of the lower stratosphere and troposphere, *J. Atmos. Sci.*, *44*, 1775–1800.
McIntyre, M. E., and T. N. Palmer (1984), The "surf zone" in the stratosphere, *J. Atmos. Terr. Phys.*, *46*, 825–849.
Mote, P. W., et al. (1996), An atmospheric tape recorder: The imprint of tropical tropopause temperatures on stratospheric water vapor, *J. Geophys. Res.*, *101*, 3989–4006.
Plumb, R. A. (1996), A "tropical pipe" model of stratospheric transport, *J. Geophys. Res.*, *101*, 3957–3972.
Plumb, R. A. (1982), The circulation of the middle atmosphere, *Aust. Meteorol. Mag.*, *30*, 107–121.
Randel, W. J., F. Wu, and D. J. Gaffen (2000), Interannual variability of the tropical tropopause derived from radiosonde data and NCEP reanalyses, *J. Geophys. Res.*, *105*, 15,509–15,523, doi:10.1029/2000JD900155.
Reed, R. J., W. J. Campbell, L. A. Rasmussen, and D. G. Rogers (1961), Evidence of downward-propagating annual wind reversal in the equatorial stratosphere, *J. Geophys. Res.*, *66*, 813–818.
Reid, G. C., and K. S. Gage (1985), Interannual variations in the height of the tropical tropopause, *J. Geophys. Res.*, *90*, 5629–5635, doi:10.1029/JD090iD03p05629.
Richter, J. H., A. Solomon, and J. T. Bacmeister (2014), On the simulation of the quasi-biennial oscillation in the Community Atmosphere Model, version 5, *J. Geophys. Res. Atmos.*, *119*, 3045–3062, doi:10.1002/2013JD021122.
Rind, D., R. Suozzo, N. K. Balachandran, A. Lacis, and G. Russell (1988), The GISS global climate–middle atmosphere model, Part I: Model structure and climatology, *J. Atmos. Sci.*, *45*, 329–370.
Rind, D., J. Jonas, N. K. Balachandran, G. A. Schmidt, and J. Lean (2014), The QBO in two GISS global climate models: 1. Generation of the QBO, *J. Geophys. Res. Atmos.*, *119*, 8798–8824, doi:10.1002/2014JD021678.
Saravanan, R. (1990), A multiwave model of the quasi-biennial oscillation, *J. Atmos. Sci.*, *47*, 2465–2474.
Scaife, A. A., et al. (2000), Realistic Quasi-Biennial Oscillations in a simulation of the global climate, *Geophys. Res. Lett.*, *27*, 3481–3484.
Schmidt, G. A., et al. (2014), Configuration and assessment of the GISS ModelE2 contributions to the CMIP5 archive, *J. Adv. Model. Earth Syst.*, *6*, 141–184, doi:10.1002/2013MS000265.
Shindell, D. T., O. Pechony, A. Voulgarakis, G. Faluvegi, L. Nazarenko, J.-F. Lamarque, K. Bowman, G. Milly, B. Kovari, R. Ruedy, and G. Schmidt (2013), Interactive ozone and methane chemistry in GISS-E2 historical and future climate simulations, *Atmos. Chem. Phys.*, *13*, 2653–2689, doi:10.5194/acp-13-2653-2013.
Strahan, S., et al. (2011), Using transport diagnostics to understand chemistry climate model ozone simulations, *J. Geophys. Res.*, *116*, D17302, doi:10.1029/2010JD015360.
Takahashi, M. (1996), Simulation of the stratospheric quasi-biennial oscillation using a general circulation model, *Geophys. Res. Lett.*, *23*, 661–664.
Veryard, R. G., and R. A. Ebdon (1961), Fluctuations in tropical stratospheric winds, *Meteorol. Mag.*, *90*, 125–143.
Wallace, J. M., and J. R. Holton (1968), A diagnostic numerical model of the quasi-biennial oscillation, *J. Atmos. Sci.*, *25*, 280–292.
Yoden, S., and J. R. Holton (1988), A new look at equatorial quasi- biennial oscillation models, *J. Atmos. Sci.*, *45*, 2703–2717.
Yudin, V. A., S. P. Smyshlyaev, M. A. Geller, and V. L. Dvortsov (2000), Transport diagnostics of GCMs and implications for 2D chemistry-transport model of troposphere and stratosphere, *J. Atmos. Sci.*, *57*, 673–699.
Zhou, X. L., M. A. Geller, and M. Zhang (2001), Tropical cold point tropopause characteristics derived from ECMWF reanalyses and soundings, *J. Clim.*, *14*, 1823–1838.
Zhou, X. L., M. A. Geller, and M. Zhang (2004), Temperature fields in the tropical tropopause transition layer, *J. Clim.*, *17*, 2901–2908.